

Basins of attraction changes by amplitude constraining of oscillators with limited power supply

S.L.T. de Souza ^a, I.L. Caldas ^a, R.L. Viana ^{b,*},
J.M. Balthazar ^c, R.M.L.R.F. Brasil ^d

^a Instituto de Física, Universidade de São Paulo, CP 66318, 05315-970 São Paulo, SP, Brazil

^b Departamento de Física, Universidade Federal do Paraná, CP 19081, 81531-990 Curitiba, Paraná, Brazil

^c Departamento de Estatística, Matemática Aplicada e Computacional, Instituto de Geociências e Ciências Exatas, Universidade Estadual Paulista, CP 178, 13500-230 Rio Claro, SP, Brazil

^d Departamento de Engenharia Estrutural e de Fundações, Escola Politécnica, Universidade de São Paulo, 05424-930 São Paulo, SP, Brazil

Accepted 1 February 2005

Abstract

We investigate the dynamics of a Duffing oscillator driven by a limited power supply, such that the source of forcing is considered to be *another* oscillator, coupled to the first one. The resulting dynamics come from the interaction between both systems. Moreover, the Duffing oscillator is subjected to collisions with a rigid wall (amplitude constraint). Newtonian laws of impact are combined with the equations of motion of the two coupled oscillators. Their solutions in phase space display periodic (and chaotic) attractors, whose amplitudes, especially when they are too large, can be controlled by choosing the wall position in suitable ways. Moreover, their basins of attraction are significantly modified, with effects on the final state system sensitivity.

© 2005 Elsevier Ltd. All rights reserved.

1. Introduction

Impact oscillators have oscillating parts colliding with other vibrating components or rigid walls [1,2]. This phenomenon is either desirable, being the basis of their operation, or is destructive and should be eliminated or, at least, suppressed to tolerable levels [3]. Usually, for applications of impact oscillators, it is important to achieve regulated periodic motion, that is, stationary periodic impact regimes. For these reasons, impact oscillator systems have been extensively investigated [4,5]. Various dynamical phenomena, like periodic and chaotic motion [6,7], bifurcations [8–10], sudden changes in attractors [11], and intermittency [12] have also been investigated in these systems. Coexisting attractors of impact oscillator and their basins of attractions, i.e., the set of initial conditions which eventually approach each particular attractor [13], have also been investigated [14,15].

* Corresponding author. Tel.: +55 44 366 2323; fax: +55 41 267236.
E-mail address: viana@fisica.ufpr.br (R.L. Viana).

The above mentioned works deal with oscillators that are driven by systems whose amplitude and frequency can be arbitrarily chosen. However, in several mechanical experiments this cannot be achieved because the forcing source has a limited available energy supply. This has been called non-ideal energy sources [16]. A common example appears when the driving comes from an unbalanced rotor linked to the oscillator, fed by an electric motor. As a consequence of this mechanical coupling, the rotor dynamics may be heavily influenced by the oscillating system being forced. As a consequence, the resulting oscillations differ from those predicted for experiments with ideal motors. Hence, the driven system cannot be considered as given a priori, but it must be taken as also a consequence of the dynamics of the whole system (oscillator plus rotor) [16–20]. This has the effect of increasing the number of degrees of freedom, when compared with ideal motors.

In this paper we will consider the Duffing oscillator driven by a limited power supply. This system can be considered, without loss of generality, as the simplest type of smooth non-linear oscillator with non-ideal driving, and can be used as a starting point for studying more complex oscillators appearing in engineering applications [22]. For this system, we initially determine coexisting periodically attractors and analyze their basins of attraction.

We also considered the impact oscillator resulting from constraining the amplitude of the forced oscillations by placing a rigid wall at a given position, such that the Duffing oscillator eventually collides with the wall. The impact process is instantaneous, with the velocity coming out of the collision being a function of the incoming velocity only. We investigate the modifications suffered from the oscillator dynamics when its amplitude is constrained in this way. It turns out that some of the attractors of the unconstrained system disappear and other are modified. In particular, by choosing conveniently some control parameters, the oscillator impacts with the wall can eliminate attractors with large vibration amplitudes. However, there may happen that some attractors survive to the collision, but their basins of attractions are significantly modified, diminishing the final state sensitivity displayed by the system.

This paper is organized as follows: In Section 2 we consider the equations for the combined Duffing oscillator with the non-ideal energy source. In Section 3 we analyze the resulting basins of attractions. Section 4 considers the effects of the collisions with a fixed hard wall on the attractors of the unconstrained system. Section 5 deals with qualitative and quantitative changes in the basin structure by considering how it affects the final state sensitivity. The last section contains our conclusions.

2. Oscillator with non-ideal excitation

In the following we will consider the one-dimensional motion of a cart of mass M connected to a fixed frame by a non-linear spring and a dashpot (viscous coefficient c) (Fig. 1(a)). The non-linear spring stiffness is given by $k_1 X - k_2 X^3$, where X denotes the cart displacement with respect to some equilibrium position in the absolute reference frame. The motion of

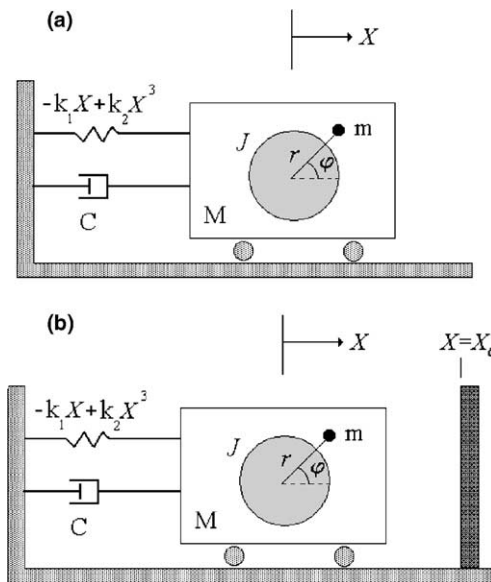


Fig. 1. (a) Schematic model of a cart driven by a motor with unbalanced mass; (b) model with a limited constraint.

the cart is due to an in-board non-ideal motor with moment of inertia J and driving an unbalanced rotor. We denote by φ the angular displacement of the rotor, modelled as a particle of mass m attached to a massless rod of radius d with respect to the rotation axis. Here E_1 is the voltage and E_2 is a characteristic parameter of the considered motor [17].

The motion of the cart is governed by the following equations [17]:

$$M \frac{d^2 X}{dt^2} + c \frac{dX}{dt} - k_1 X + k_2 X^3 = mr \left[\frac{d^2 \varphi}{dt^2} \sin \varphi + \left(\frac{d\varphi}{dt} \right)^2 \cos \varphi \right], \tag{1}$$

$$(J + mr^2) \frac{d^2 \varphi}{dt^2} = mr \frac{d^2 X}{dt^2} \sin \varphi + E_1 - E_2 \frac{d\varphi}{dt}. \tag{2}$$

It is convenient to work with dimensionless positions and time, according to

$$X \rightarrow x \equiv \frac{X}{r}, \tag{3}$$

$$Y \rightarrow y \equiv \frac{Y}{r}, \tag{4}$$

$$t \rightarrow \tau \equiv t \sqrt{\frac{k_1}{M}}, \tag{5}$$

in such a way that Eqs. (1) and (2) are rewritten in the following form

$$\ddot{x} + \beta \dot{x} - x + \delta x^3 = \epsilon_1 (\ddot{\varphi} \sin \varphi + \dot{\varphi}^2 \cos \varphi), \tag{6}$$

$$\ddot{\varphi} = \epsilon_2 \ddot{x} \sin \varphi + E_1 - E_2 \dot{\varphi}, \tag{7}$$

where the dots stand for differentiation with respect to the scaled time τ , and the following abbreviations were introduced:

$$\beta \equiv \frac{c}{\sqrt{k_1 M}}, \quad \delta \equiv \frac{k_2}{k_1} r^2, \quad \epsilon_1 \equiv \frac{m}{M}, \tag{8}$$

$$\epsilon_2 \equiv \frac{mr^2}{J + mr^2}, \quad E_1 \equiv \frac{E_1 M}{k_1 (J + mr^2)}, \quad E_2 \equiv \frac{E_2}{J + mr^2} \sqrt{\frac{M}{k_1}}. \tag{9}$$

3. Basins of attraction

The phase space of the combined Duffing-rotor system has out of four dimensions, but we will be chiefly interested in the position of the oscillator itself, since its collisions with the wall will be determined by the mutual distance between the oscillator and the constraint. Hence, we will focus on the displacement x of the Duffing oscillator. Throughout the paper we will fix the values of all (scaled) parameters $\beta = 0.02$, $\delta = 0.1$, $\epsilon_1 = 0.1$, $\epsilon_2 = 0.25$, and $E_2 = 1.5$; such that the control parameter we choose to work with is related with the strength of the motor E_1 .

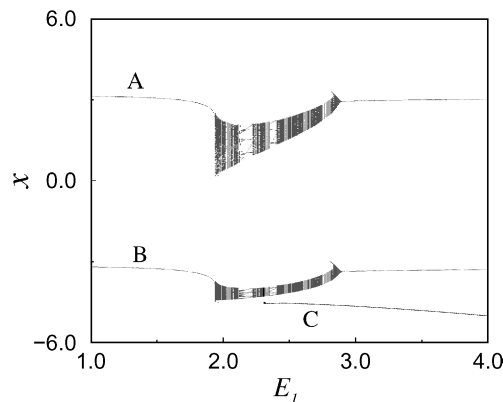


Fig. 2. Bifurcation diagram showing three attractors of the cart displacement without impacts as a function of the control parameter E_1 .

In Fig. 2 we show a bifurcation diagram in terms of the cart displacement x , registered each time the cart velocity reaches a null velocity, versus the control parameter E_1 . If its value is below a certain threshold $E_{1C} \approx 1.9$, there are two coexisting periodic attractors, named as A and B , representing small limit-cycles in the $x - \dot{x}$ projection of the phase space (see Fig. 3(a)). For $E_1 > E_{1C}$ chaotic motion sets in, one chaotic band for each attractor, interspersed with windows of periodic motion. After $E_{1X} \approx 2.3$ a third and periodic attractor, named as C , evolves, as a large amplitude limit cycle shown in Fig. 3(b). At $E_{1F} \approx 2.8$ the chaotic bands become quasi-periodic attractors and, increasing further the value of E_1 , periodic attractors at approximately the same phase space location of A and B , and the third attractor C seems not to be noticeably affected.

From the engineering point of view, if the Duffing oscillator represents a lowest-order approximation of some non-linear vibrating system under a non-ideal forcing, it may be desirable to avoid the large-amplitude attractor C , since it can drive the oscillator off its bearings or guides. Hence, it turns out to be better to tune its operation so as to yield one of the two small-amplitude attractors (A or B), depending on the initial condition chosen.

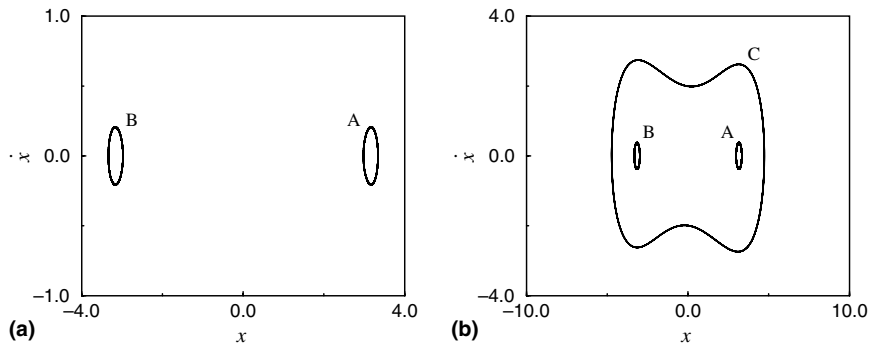


Fig. 3. Velocity versus displacement of the cart. (a) Two periodic attractors for $E_1 = 1.70$; (b) Three periodic attractors for $E_1 = 3.25$.

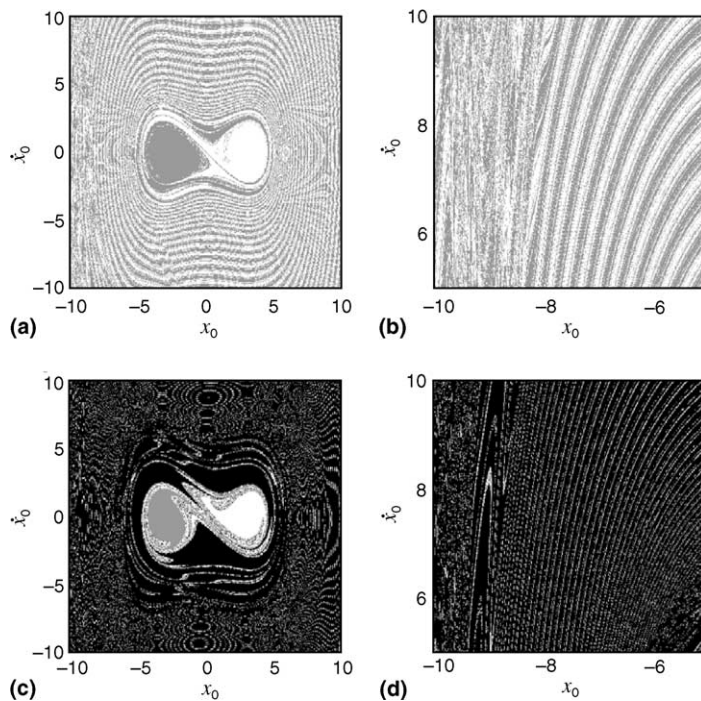


Fig. 4. Basins of attraction, (a) for the two periodic attractors A (white) and B (gray) shown in Fig. 3(a), (b) magnification of previous figure, (c) for the three periodic attractors A (white), B (gray), C (black) shown in Fig. 3(b), (d) magnification of previous figure.

In any case it is of practical importance to investigate the basins of attraction related to A , B and C , since we can determine to what extent a small uncertainty in the initial condition reflects on the knowledge of the attractor the system will asymptote to. Fig. 4(a) shows the basins of attractions, for the attractors A (white) and B (gray) considered in Fig. 3(a). Its overall structure resembles that occurring for the Duffing oscillator driven by an ideal source (unlimited power supply) of the form $f_0 \cos(\omega t)$ [23]. There are two lobes corresponding to those observed for the free motion, but their boundary seems to be no longer a smooth curve, but it presents fractal incursions into the lobes, especially near the unstable equilibrium point at the origin $(0,0)$. The involved nature of the accumulation of the basin bands is more evident in Fig. 4(b), where a small box picked up from Fig. 4(a) is magnified.

Fig. 4(c) shows a similar situation, but for a control parameter value at which there are three coexisting attractors, with their corresponding basins being depicted in white (A), gray (B), and black (C), respectively. In this case the fractal nature of the basin boundary is more evident, in particular when a magnification is made (Fig. 4(d)). The quantitative consequences of this basin structure will be dealt with in Section 5.

4. Unilateral amplitude constraints

In this section, we take into account the effect of the impact constraints on the attractors and their basins of the studied system. Applications of vibrating systems often present amplitude limitations imposed by their design or by safety reasons. For example, a vibrating rod has typically some clearance, or gap with respect to other moving or fixed element, with the purpose of lubrication and accommodation of thermal expansion. These gaps represent amplitude constraints since the oscillating system experience collisions, which will be modelled as a rigid wall placed at a fixed position x_c (Fig. 1(b)).

We model the collisions with the wall by the laws of inelastic impact: the velocity after the impact is taken to be $-R$ times the velocity before the impact, where R is the restitution coefficient. The numerical integration is done for the system until it reaches $x = x_c$, when we stop the integration and reset variables so that the position is reinitialized at x_c , but the velocity is initialized according to the rule mentioned above.

We use $R = 0.9$ in the following simulations. In order to facilitate the analysis, we depict in gray the corresponding attractors without amplitude constraints. Fig. 5 shows a bifurcation diagram for the oscillator position as a function of the control parameter E_1 , in presence of a rigid wall placed at $x_c = 3.4$ (Fig. 5(a)) and 4.1 (Fig. 5(b)), in order to study the alterations on the coexisting attractors caused by the amplitude constraint. It alters the system attractor topology, destroys some attractors, and originates other new ones, whereas other attractors are not altered. The possible alteration depends on the control parameters of the unperturbed system as well as the amplitude constraint position.

In Fig. 5(a), we observe that the former attractors A and B are barely modified, but A undergoes a bifurcation cascade leading to a tiny chaotic region, and goes back to a periodic attractor, thus the impacts have suppressed one of the chaotic bands (shown in gray for comparison). Moreover, the large-amplitude attractor, now denoted as D , appears in the left hand side of the origin. This is not at all equivalent to the attractor C observed before, since the system does not have an exact symmetry $x \rightarrow -x$ (the chaotic bands, for example, are different even in the absence of amplitude constraints). The chaotic band is not destroyed at all for a different value of x_c , as illustrated by Fig. 5(b), and there (at least) are two more periodic attractors, C and E , born at different intervals of the control parameter E_1 .

To evaluate the basins of attraction alterations on the remaining attractors, we present in Fig. 6(a) the new basins for the attractors A and B of Fig. 5(a) and, in Fig. 6(b), a magnification of a small box containing these basins. The amplitude constraint limits the initial conditions that can be considered. Comparing with the magnification shown

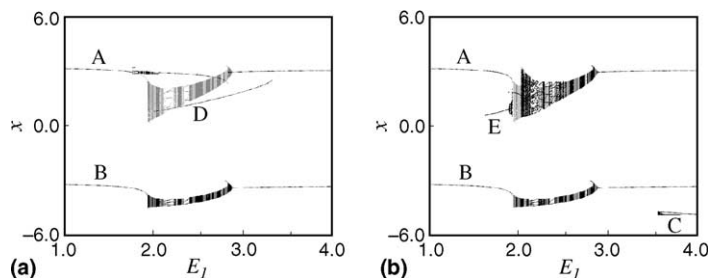


Fig. 5. Bifurcation diagrams showing the attractors of the cart displacement as a function of the control parameter E_1 . (a) For $x_c = 3.4$ and (b) $x_c = 4.1$. In gray is shown the attractors without impacts (the same are labelled A in Fig. 2).

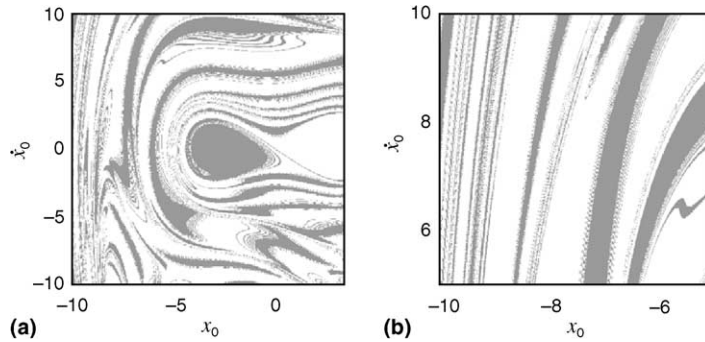


Fig. 6. (a) Basins of attraction of the two periodic attractors A (white) and B (gray) shown in Fig. 5(a) for $x_c = 3.4$ and (b) their magnification.

in Fig. 4(b), the magnified new basins show the presence of thicker bands of initial conditions that asymptote to the same attractor.

An example of how the attractor basin is modified by the amplitude constraint is shown in Fig. 7(a), which presents the displacement evolution, without the constraint, for a given initial condition that belongs to the A -attractor basin. Fig. 7(b) shows this situation with a constraint, this same initial condition being now located at the B -attractor basin. The corresponding phase-space projection trajectories, for this initial condition, are shown in Fig. 7(c) and (d), respectively. Hence, successive collisions of the Duffing oscillator steers the phase space trajectory from A to B attractor.

The periodic attractors A , B , and E of Fig. 5(b) are shown in phase space in Fig. 8. The third attractor E is still a large-amplitude one, as compared with A and B , but it nevertheless is bounded by the amplitude constraint, what can be seen in the flatness of the limit-cycle at the wall position x_c . Their basin structure is also very involved, what is illustrated

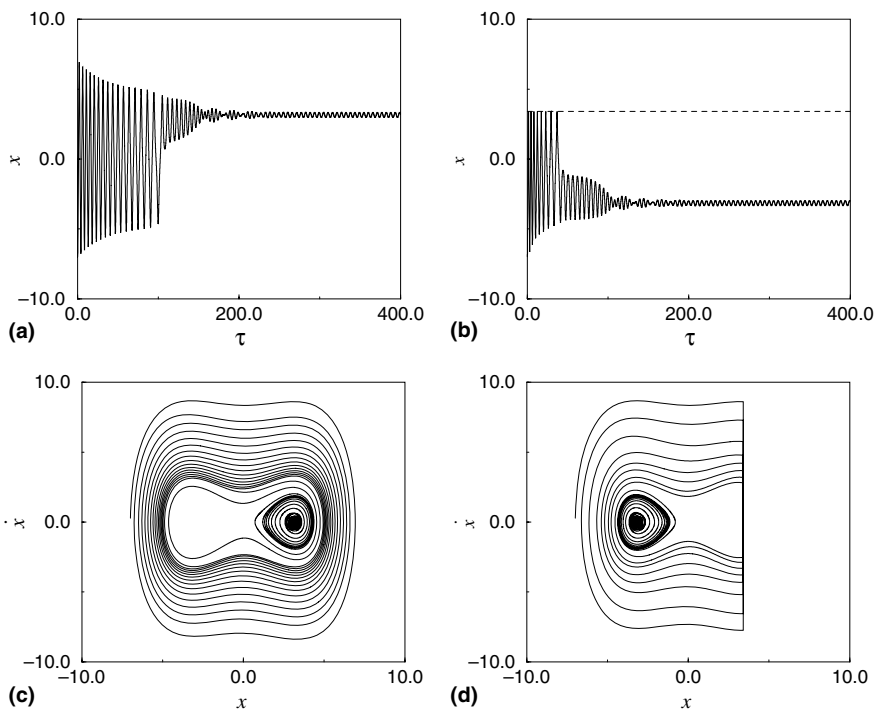


Fig. 7. Displacement versus time of the attractors A and B shown in Fig. 3(a); (a) attractor A without impacts; (b) attractor B with impacts (at $x_c = 3.4$, dashed line) during the transient regime, (c) and (d) shows the corresponding phase space trajectories of (a) and (b), respectively.

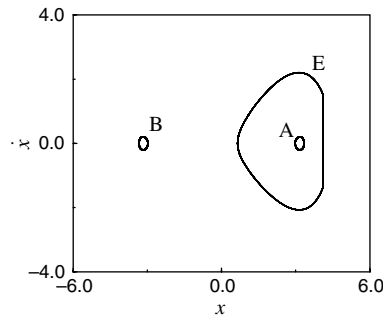


Fig. 8. Velocity versus displacement of the cart for three periodic attractors at $E_1 = 1.7$ and $x_c = 4.1$.

by Fig. 9, which shows these attractors basins (Fig. 9(a)) and a magnification (Fig. 9(b)). In this example, a new attractor appears due to the constraint. Therefore, although the new basin bands are broader than in the case without constraint, we have in this case the competition of a new third attractor with its thin basin bands, what deranges the final state prediction.

The next example shows another kind of basin modifications that, for some control parameters, may be introduced by the constraint whenever an attractor with a large amplitude oscillation disappears (as the attractor C in Fig. 3(b)). Thus, in Fig. 10 we see the new basins for the remaining attractors A and B , after the attractor C has been destroyed.

Comparing Figs. 10(b) and 4(d), we conclude that the basin of attraction structure becomes more complex when there are amplitude constraints on the motion. Moreover, Fig. 11 shows the transient trajectory of attractor E , without constraint (Fig. 11(a)), and how the attractor is not accessible due to the wall collisions (Fig. 11(b)).

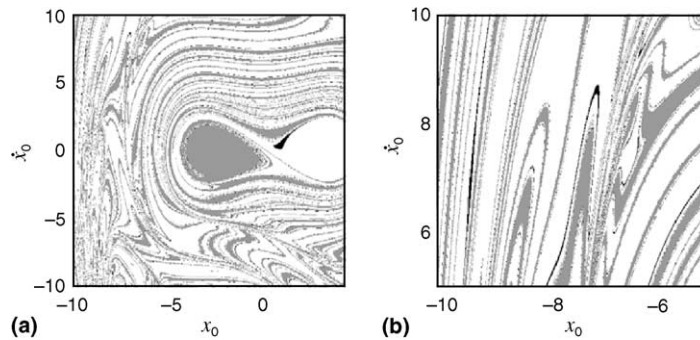


Fig. 9. (a) Basins of attraction of the two periodic attractors A (white), B (gray), and E (black) shown in Fig. 8 and (b) their magnification.

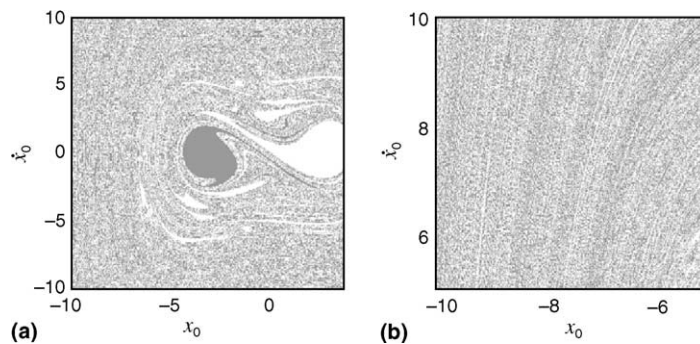


Fig. 10. (a) Basins of attraction of the two periodic attractors A (white) and B (gray) shown in Fig. 3(b) for $x_c = 4.1$ and (b) their magnification.

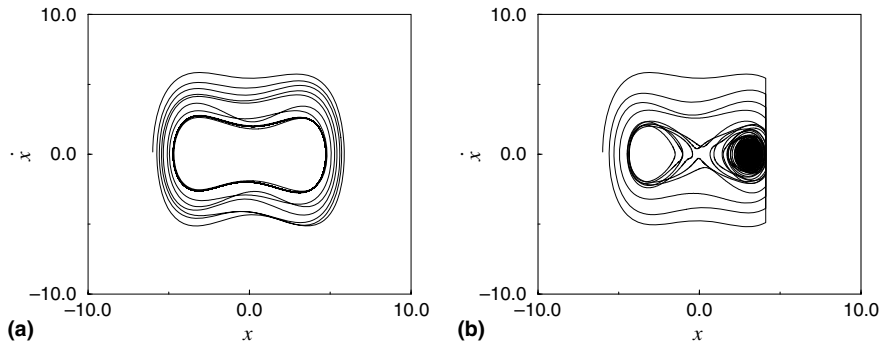


Fig. 11. Phase space trajectories corresponding to the attractor E of Fig. 5(b). (a) Without constraints, (b) with a constraint at $x_c = 4.1$.

5. Final state sensitivity

To evaluate the final state sensitivity we calculate the fraction of uncertain initial conditions in phase space, in order to estimate the probability of making a wrong prediction about to what attractor will a given trajectory asymptote to, given a small uncertainty ϵ . It is well-known that, for smooth basin boundaries, this fraction scales linearly with ϵ , so that for getting better predictions about the final state one simply has to improve the precision on determining the initial conditions, i.e., reducing their uncertainty ϵ . On the other hand, if the basin boundary is fractal, this scaling is a power law with an exponent between 0 and 1, implying that even a great reduction of ϵ has a poor effect on improving the knowledge of the final state. This has been called *final state sensitivity* by Grebogi and his collaborators in a series of seminal papers [24,25].

Figs. 4(b) and 6(b) are magnification of basin segments of two coexisting attractors A and B , without and with amplitude constraints respectively, so that one can assess to what extent this affects the final state sensitivity of the system. In both cases we choose randomly a large number of initial conditions and, for each one, we have constructed a ball of radius ϵ . Two other nearby initial conditions are chosen within this small ball, and we compare whether or not the resulting trajectories asymptote to the same attractor (either A or B). If one of the perturbed trajectories fails to asymptote to the same attractor, this initial condition is dubbed as uncertain within an accuracy ϵ .

By considering a large number of initial conditions, we can estimate the fraction of ϵ -uncertain points in the box, $f(\epsilon)$. This number scales with the uncertainty radius as a power-law $f(\epsilon) \sim \epsilon^\eta$, where η is called uncertainty exponent [25]. Since the underlying phase space is two-dimensional, it turns out that the box-counting dimension of the projection of the basin boundary is $D = 2 - \eta$. If $\eta = 1$, i.e., the uncertain fraction scales linearly with the uncertain radius, it follows that the basin boundary is a smooth curve, since $D = 1$. On the other hand, if $0 < \eta < 1$, the basin boundary projection has a fractal dimension between 1 and 2.

Our results are shown in Fig. 12 for the uncertain fraction versus the radius of an uncertainty ball for the basins of Figs. 4(b) (solid line) and 6(b) (dashed line). In both cases we have verified the power-law scaling characteristic of fractal

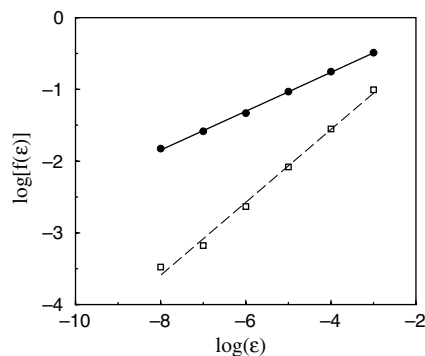


Fig. 12. Uncertain fraction versus ϵ for the basin boundary region depicted in Figs. 4(b) (solid line) and 6(b) (dashed line). The lines are least squares fits, with slopes 0.27 ± 0.01 (solid line) and 0.51 ± 0.02 (dashed line).

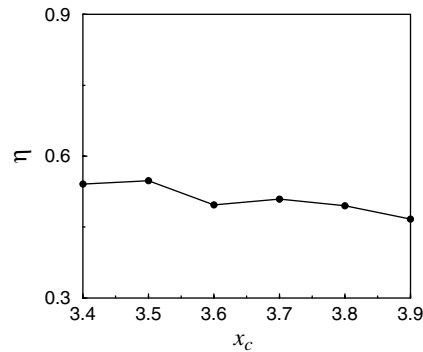


Fig. 13. Uncertainty exponent η as a function of the amplitude constraint position x_c .

basin boundaries, with uncertainty exponents given by $\eta = 0.27 \pm 0.01$ for the solid line (without constraint) and $\eta = 0.51 \pm 0.02$ for the dashed line (with amplitude constraint). Since the closer the exponent η is from zero the more involved is the basin boundary, in this case at least the introduction of an amplitude constraint has decreased the final state sensitivity or, in other words, improved the prediction about to what attractor the system will converge to, up to a given uncertainty. However, the value of the uncertainty exponent seems also to vary with the position of the wall x_c , as illustrated in Fig. 13, where the uncertainty exponent η is plotted against x_c .

6. Conclusion

The introduction of amplitude constraints, modelled as a rigid wall which collides with the vibrating system, is shown to modify in a large extent its dynamics. The constraint is able to suppress or modify the topology of the attractors, destroying chaotic attractors or creating new periodic and chaotic attractors. It also limits the amplitude of certain attractors, which is a natural effect of constraining the oscillator motion. However, even in the case the attractors are not much modified by the constraint, their basins of attraction may be significantly modified.

Another effect of the amplitude constraint is to modify the basin boundary structure. We have observed situations in which the final state sensitivity decreases with introduction of the constraint, but this may depend on other parameters of the system, and a more comprehensive analysis would be necessary to map all the possibilities. Our analysis have been mainly numerical, since this is a non-smooth system to which many available analytical methods fail to apply.

Acknowledgments

This work was made possible by partial financial support from the following Brazilian government agencies: FAPESP, CAPES, and CNPq.

References

- [1] Blazejczyk-Okolewska B, Czolczynsky K, Kapitaniak T, Wojewoda J. *Chaotic mechanics in systems with friction and impacts*. Singapore: World Scientific; 1999.
- [2] Blazejczyk-Okolewska B, Czolczynsky K, Kapitaniak T. Classification principles of types of mechanical systems with impacts—fundamental assumptions and rules. *Euro J Mech A/Solids* 2004;23(3):517–37.
- [3] Czolczynsky K. On the existence of a stable periodic solution of an impacting oscillator with damping. *Chaos, Solitons & Fractals* 2004;19:1291–311.
- [4] Nordmark AB. Non-periodic motion caused by grazing incidence in an impact oscillator. *J Sound Vibrat* 1991;145:279–97.
- [5] Karagiannis K, Pfeiffer F. Theoretical and experimental investigations of gear-rattling. *Nonlinear Dyn* 1991;2:367–87.
- [6] Li G-X, Rand RH, Moon FC. Bifurcations and chaos in a forced zero-stiffness impact oscillator. *Int J Non-Linear Mech* 1990;25:417–32.
- [7] Luo GW. Period-doubling bifurcations and routes to chaos of the vibratory systems contacting stops. *Phys Lett A* 2004;323:210–7.

- [8] Aidanpää J-O, Shen HH, Gupta RB. Stability and bifurcations of a stationary state for an impact oscillator. *Chaos* 1994;4:621–30.
- [9] Dankowicz H, Piironen P, Nordmark AB. Low-velocity impacts of quasi-periodic oscillations. *Chaos, Solitons & Fractals* 2002;14:241–55.
- [10] Nordmark AB. Effects due to low-velocity impacts in mechanical oscillations. *Int J Bifurcat Chaos* 1992;2:597–605.
- [11] de Souza SLT, Caldas IL, Viana RL, Balthazar JM. Sudden changes in chaotic attractors and transient basins in a model for rattling in gearboxes. *Chaos, Solitons & Fractals* 2004;21:763–72.
- [12] Peterka F, Kotera T, Cibera S. Explanation of appearance and characteristics of intermittency chaos of the impact oscillator. *Chaos, Solitons & Fractals* 2004;19:1251–9.
- [13] Blazejczyk-Okolewska B, Brindley J, Kapitaniak T. Practical riddling in mechanical systems. *Chaos, Solitons & Fractals* 2000;11:2511–4.
- [14] Isomäki HM, Von Boehm J, Rätty R. Fractal basin boundaries of an impacting particle. *Phys Lett A* 1988;126:484–90.
- [15] Blazejczyk-Okolewska B, Kapitaniak T. Co-existing attractors of impact oscillator. *Chaos, Solitons & Fractals* 1998;9:1439–43.
- [16] Kononenko VO. *Vibrating systems with a limited power supply*. London: Iliffe Books Ltd; 1969.
- [17] Warminski J, Balthazar JM, Brasil RMLRF. Vibrations of a non-ideal parametrically and self-excited model. *J Sound Vibrat* 2001;245:363–74.
- [18] Dimentberg MF, McGovern L, Norton RL, Chapdelaine J, Harrison R. Dynamics of an un-balanced shaft interacting with a limited power supply. *Nonlinear Dyn* 1997;13:171–87.
- [19] Krasnopolskaya TS, Shvets AY. Chaos in vibrating systems with a limited power-supply. *Chaos* 1993;3:387–95.
- [20] de Souza SLT, Caldas IL, Viana RL, Balthazar JM, Brasil RMLRF. Impact dampers for controlling chaos in systems with limited power supply. *J Sound Vibrat* 2005;279:955–67.
- [22] Nayfeh AH, Mook DT. *Nonlinear oscillations*. New York: Wiley-Interscience; 1979.
- [23] Mitić S. Dynamics of the Duffing oscillator with impacts. *Facta Universitatis* 1997;1:65–72.
- [24] McDonald SW, Grebogi C, Ott E. Fractal basin boundaries. *Physica D* 1985;17:125–53.
- [25] McDonald SW, Grebogi C, Ott E. Final state sensitivity: An obstruction to predictability. *Phys Lett A* 1983;99:415–8.